REFERENCES

1. Silverberg E, Lubera JA. Cancer statistics, 1989. *Cancer* 1989;39:3–20.
2. Laramore GE. Head and neck cancer: a general overview. In: Laramore GE, ed. *Radiation therapy of head and neck cancer*. New York: Springer-Verlag; 1989: 1–11.
3. Myers EM. *Head and neck oncology. Diagnosis, treatment and rehabilitation*. Boston: Little, Brown and Co.; 1991.
4. Shear M, Hawkins DM, Farr HW. The prediction of lymph node metastases from oral squamous carcinomas. *Cancer* 1976;37:1901–1907.
5. Brekel van den MW, Stel HV, Casteljins JA, et al. Cervical lymph node metastasis: assessment of radiologic criteria. *Radiology* 1990;177:379–384.
6. Brekel van den MW, Casteljins JA, Croll GA, et al. Magnetic resonance imaging versus palpation of cervical lymph node metastasis. *Arch Otolaryngol Head Neck Surg* 1991;117:666–673.
7. Feinmesser R, Freeman JL, Noyek AM, Birt D, Gullane P, Mullen JB. MRI and neck metastases: aclinical, radiological pathological correlative study. *J Otolaryngol* 1990; 19:136–140.
8. Hillshamer PJ, Schuller DE, McGhee RB Jr, Chakeres D, Young DC. Improving diagnostic accuracy of cervical metastases with computed tomography and magnetic resonance imaging. *Arch Otolaryngol Head Neck Surg* 1990;119:1297–1301.
9. Mancuso AA, Harnsberger HR, Muraki AS, Stevens MH. Computed tomography of cervical and retropharyngeal lymph nodes: normal, and applications in staging head and neck cancer. Part I: normal anatomy. *Radiology* 1983;148:709–714.
10. Mancuso AA, Harnsberger HR, Muraki AS, Stevens MH. Computed tomography of cervical and retropharyngeal lymph nodes: normal, and applications in staging head and neck cancer. Part II: pathology. *Radiology* 1983;148:715–723.
11. Stark DD, Moss AA, Gamsu G, Clark OH, Gooding GA, Webb WR. Magnetic resonance imaging of the neck. Part I: normal anatomy. *Radiology* 1984;150:447–454.
12. Stark DD, Moss AA, Gamsu G, Clark OH, Gooding GA, Webb WR. Magnetic resonance imaging of the neck. Part II: pathology. *Radiology* 1984;150:455–461.
13. Stern WB, Silver CE, Zeifer BA, Persky MS, Heller KS. Computed tomography of the clinically negative neck. *Head and Neck* 1990;12:109–113.
14. Baum RP, Hertel A, Lorenz M, Encke A, Hör G. Technetium-99m-labeled anti-CEA monoclonal antibodies for tumor immunoscintigraphy. *Nucl Med Commun* 1989;10: 345–352.
15. Samuel J, Noujaim AA, Willans DJ, Brzezinska GS, Haines DM, Longenecker BM. A novel marker for basal (stem) cells of mammalian stratified squamous epithelia and squamous-cell carcinomas. *Cancer Res* 1989;49:2465–2470.
16. McEwan AJB, MacLean GD, Hooper HR, et al. MAb-170H.82: an evaluation of a novel panadenocarcinoma monoclonal antibody labeled with ^{99m}Tc and ^{111}In. *Nucl Med Commun* 1992;13:11–19.
17. Baum RP, Adams S, Kiefer J, et al. A novel technetium-99m-labeled monoclonal antibody (174H.64) for staging head and neck cancer by immuno-SPECT. *Acta Oncol* 1993;32:747–751.
18. Schomburg A, Hotze AL, Walther EK, Alberty J, Bender H, Herberhold C, Biersack HJ. Radioimmunoimaging of head and neck cancer. *Onkologie* 1993;16:465–469.
19. Amdur RJ, Parsons JT, Mendenhall WM, Million RR, Stringer SP, Cassisi NJ. Postoperative irradiation for squamous-cell carcinoma of the head and neck: an analysis of treatment results and complications. *Int J Radiat Oncol Biol Phys* 1989;16:25–36.
20. Coman RE. Single-photon emission computed tomography and positron emmision tomography in cancer imaging. *Cancer* 1991;67:1261–1270.
21. Links JM. Multidetector single-photon emission tomography: are two (or three or four) heads really better than one? *Eur J Nucl Med* 1993;20:440–447.
22. Baatenburg de Jong RJ, Rongen RJ, Lameris JS, Harthoorn M, Verwoerd CD, Knegt R. Metastatic neck disease. Palpation versus ultrasound examination. *Arch Otol Head Neck Surg* 1989;115:689–690.
23. Kabala L, Goddard P, Cook P. Magnetic resonance imaging of extracranial head and neck tumors. *Br J Radiol* 1992;65:375–383.
24. Badcock PC. The role of computed tomography in the planning of radiotherapy fields. *Radiology* 1983;147:241–244.
25. Zum Winkel K, Hermann HJ. Computerized tomography in radiation treatment planning. In: Gerhardt P, Kaick GV, eds. *Total-body computed tomography*. Stuttgart: Thieme Verlag; 1979:232–241.
26. Aspestrand F, Kolbenstvedt A, Boysen M. Carcinoma of the hypopharynx: CT staging. *J Comp Assist Tomogr* 1990;14:72–76.
27. de Bree R, Roos JC, Quak JJ, et al. Clinical imaging of head and neck cancer with technetium-99m-labeled monoclonal antibody E48 IgG or F(ab')$_2$. *J Nucl Med* 1994;35:775–783.
28. van Dongen G A, Leverstein H, Roos JC, et al. Radioimmunoscintigraphy of head and neck cancer using Tc-99m-labeled monoclonal antibody E48 F(ab')$_2$. *Cancer Res* 1992;52:2569–2574.
29. Larson SM. Radiolabeled monoclonal anti-tumor antibodies in diagnosis and therapy. *J Nucl Med* 1985;26:538–545.
30. Laubenbacher C, Saumweber D, Avril N, et al. Prospective evaluation of MRI and ^{18}F-FDG PET for staging of squamous-cell carcinomas of the head and neck [Abstract]. *J Nucl Med* 1995;36(suppl):221P.
31. Anzai Y, Carroll WR, Bradford CR, Wolf GT, Wahl RL. Prospective comparison of FDG-PET and MRI in the diagnosis of post-surgery/radiation recurrence of head and neck cancer [Abstract]. *J Nucl Med* 1995;36(suppl):221P.
32. Snow GB, Patel P, Leemans CR, Tiwari RL. Management of cervical lymph nodes in patients with head and neck cancer. *Eur Arch Otorhinolaryngol* 1992;249:187–194.

Ictal Cerebral Blood Flow in Seizures Originating in the Posterolateral Cortex

R. Duncan, S. Rahi, A.M. Bernard, A. Biraben, A. Devillers, J. Lecloirec, J.P. Vignal and P. Chauvel

Neurology Clinic, University of Rennes Regional Medical Center, and Department of Nuclear Medicine, Centre Eugène Marquis, Rennes, France

In selecting patients for epilepsy surgery, it is important to distinguish mesial temporal seizures from seizures originating in the posterolateral cortex. We studied ictal cerebral perfusion in five patients with complex partial seizures with clear posterior EEG ictal onsets and clinical seizure semiology suggesting seizure origin in the posterolateral cortex. **Methods:** Ictal SPECT was performed during video EEG monitoring using ^{99m}Tc-HMPAO as a cerebral perfusion tracer and a rotating gamma camera to acquire images. **Results:** Three patterns of ictal hyperperfusion were seen: pattern A = temporoparieto-occipital junction extending into the lateral temporal cortex, involving the mesial temporal cortex and basal ganglia to a lesser degree and a small area of hyperperfusion in the contralateral parietal cortex (two patients); pattern B = pattern A but with no hyperperfusion of the mesial temporal cortex (one patient); and pattern C = localized hyperperfusion in the area of the temporoparieto-occipital junction (two patients). **Conclusion:** Our results suggest distinct patterns of ictal perfusion in seizures with posterolateral ictal EEG onsets. Ictal SPECT may be useful in distinguishing such seizures.

Key Words: cerebral blood flow; epilepsy; temporoparieto-occipital junction seizures; localization

J Nucl Med 1996; 37:1946–1951

Ictal HMPAO-SPECT has been used as a localizing investigation in partial epilepsies, particularly those of mesial temporal lobe origin, where studies have shown accurately localizing changes in a high proportion of cases (*1–19*). The pattern of perfusion change seen during seizures originating in the mesial temporal lobe (*2,3,8,11,13*) shows hyperperfusion of the entire anterior temporal lobe, including the mesial and lateral cortices. This hyperperfusion could extend into the ipsilateral basal ganglia and involve the contralateral temporal lobe. The rest of the ipsilateral hemisphere is hypoperfused. Fewer data exist on postictal patterns of perfusion in extratemporal seizures (*15–19*), but it has been suggested that early injection of HMPAO can detect changes in rCBF, which can produce useful localizing information (*19*).

Received Dec. 5, 1995; revision accepted Apr. 10, 1996.

For correspondence or reprints contact: R. Duncan, MD, PhD, MRCP, Dept. of Neurology, Institute of Neurological Sciences, Southern General Hospital, Glasgow G51 4TF, Scotland.

Seizures of the posterolateral cortex in the area of the temporoparieto-occipital junction are not extensively described in the literature. Because limbic structures are sometimes involved early by propagation of the ictal discharge, seizures in this area are sometimes difficult to distinguish from those of mesial temporal origin (*20*), although ictal discharges in our patients had clear posterior onsets. Temporoparieto-occipital junction seizures are characterized by early clinical features of involvement by seizure discharges of neighboring areas of the temporal, parietal and occipital lobes, such as, vertiginous sensations (*20*), visual hallucinations (*21*), head and truncal version gyration (*22,23*) and oculoclonus and rapid blinking (*20*). Further seizure features suggesting mesial temporal propagation, such as oro-alimentary and gestural automatisms (*23,24*), occur. Long-lasting postictal aphasia is also seen. As surgical treatment is not often contemplated in such patients, invasive EEG localizing data and its confirmation by a successful resection are not usually available. The detection of these seizures is nonetheless important. Standard temporal lobe resections (anterior temporal lobectomy, amygdalo-hippocampectomy) are unlikely to affect temporoparieto-occipital junction seizures, and the seizure area itself is not amenable to resection on the dominant side.

We present ictal HMPAO-SPECT data with EEG and clinical correlations in five patients with clear posterior ictal EEG onsets. We also note the clinical ictal features that suggested seizure origin in the area of the temporoparieto-occipital junction.

MATERIALS AND METHODS

Patients

All five patients (3 men, 2 woman, age range 14–38, mean age 29.2 yr) had complex partial seizures refractory to medical treatment. They were studied while having video EEG monitoring as part of their assessment for possible surgical treatment. Patient selection was based on whether clear ictal EEG onset in the posterior temporal or inferior parietal leads was present.

Clinical, EEG and imaging data are summarized in Table 1. All patients had full clinical and psychometric assessment, MRI with coronal and axial T1 and T2 slices in temporal lobe orientation, multiple and prolonged surface interictal EEG recordings, and at least 5 days of daytime video EEG monitoring. Nineteen monopolar channels of EEG were recorded using a system which allowed retrospective filtering and reformatting of the signal into any montage. EEG and video data were analyzed independently to the SPECT results. All patients had clear posterior seizure onsets on surface ictal EEG before the development of clinical features of the seizure.

Three patients had initial ictal clinical features suggestive of involvement of posterior cortex: truncal version (one patient), audiovisual hallucination followed by truncal version (one patient) and palpebral and ocular clonus (one patient). One patient had postictal aphasia which lasted approximately ten times as long as the seizure (typical seizure duration 2–3 min). No patient had ictal semiological features suggestive of mesial temporal lobe seizure origin (e.g., abdominal aura, oro-alimentary automatisms).

Three patients had posteriorly distributed interictal epileptiform abnormalities. One patient had bilateral temporal interictal discharges and the other had unilateral midtemporal discharges. One patient had an area of cortical dysplasia on MRI in the area of the temporoparieto-occipital junction. MRI was normal in the other four patients, and none of the patients had any abnormality of signal or structure in the mesial temporal structures. No incongruent localizing data were seen in this study.

Interictal SPECT

Patients were administered 740 MBq ^{99m}Tc-HMPAO, which had been reconstituted immediately beforehand, while in the supine position with their eyes closed in a quiet room. Image acquisition was performed using a gamma camera with a high-resolution, low-energy collimator; 64 planar images were acquired in a 128 × 128 matrix, each over 30 sec, giving a total acquisition time of 32 min. An average of 40,000 counts per image were acquired. The images were reconstructed in three dimensions using a Butterworth 4/16 filter with appropriate cutoff. The injection was performed more than 24 hr from the last seizure.

Ictal SPECT

Technetium-99m-pertechnetate was placed in a shielded container with a vial of HMPAO in proximity to the patients, who were under observation in the monitoring unit. On observing electrical and clinical ictal manifestations, the technologist summoned the doctor who quickly mixed the [^{99m}Tc]pertechnetate and the HMPAO and injected the compound through a preinserted intravenous catheter. The patient was then transferred to the SPECT unit and image acquisition was performed as detailed above within 1 hr of injection.

Visual Analysis of Images

Images were analyzed independently by two investigators blind to all data except the diagnosis of epilepsy. Interictal and ictal images were initially analyzed separately, and ictal changes were then assessed using both image sets. In assessing images, account was taken not only side-to-side asymmetries but the relationships between the ipsilateral structures. Images were analyzed onscreen as part of a three-dimensional dataset that could be resliced in any plane.

Numeric Analysis of Images

Datasets were transferred to a Macintosh computer and analyzed using the SME Neuro 900 image analysis software (Strichmann Medical Systems, Ltd.). Ictal and interictal images were coregistered. Predrawn templates of symmetric regions of interest (ROIs) were placed on images according to signal profiles as follows: medial frontal, inferior, intermediate and superior lateral frontal, mesial temporal, anterior lateral temporal, inferior and superior posterior lateral temporal, parietal, medial and lateral occipital and basal ganglia and cerebellar. Asymmetry indices (AI) were calculated using the following formula:

$$AI = 100 \times (L\text{-}R)/((L + R)/2). \qquad \text{Eq. 1}$$

The index is positive when the count density is greater on the left. For ictal images, percentage change in AI with respect to the interictal image was calculated. In addition to measurements using predetermined ROIs, a 10-pixel square ROI was placed according to measured signal profile over the area of maximal signal in each ictal scan. AI was calculated with reference to the homotopic contralateral cortex and compared with the same areas on the coregistered interictal scan.

RESULTS

The results of HMPAO-SPECT are summarized in Table 1. Ictal percentage change in AI with respect to the interictal image is shown in Table 2.

According to visual analysis, Patient 1, whose interictal scan was obtained 48 hr after the ictal scan, with no intervening seizures, had localized hypoperfusion of the left mesial temporal lobe and hyperperfusion of the posterior lateral cortex. These abnormalities were associated with mesial and lateral temporal asymmetry indices of 6.2% and 12.4%, respectively. The patient also had a cerebellar AI of 10.9%, although asymmetry was not noted visually by the observers. In Patient 4, there was

TABLE 1
Clinical, MRI and EEG Localizing Data: Results of Interictal and Ictal SPECT

Patient no.	MRI	Seizure semiology	Interictal EEG
1	Normal	Initial tonic grimace with head and truncal version No aura	L mid temporal spikes
2	Cortical dysplasia posterolateral temporal cortex	Initial complex audio-visual hallucination, then head and truncal version. Postictal aphasia	L posterior T spike and slow
3	Normal	Initial palpebral clonus and nystagmoid ocular deviation No aura	L TP sharp and slow wave discharges
4	Normal	Initial tonic grimace and mastication Nonspecific aura	Bilateral TPO sharp and slow waves
5	Normal	Massive postictal aphasia No aura	Bitemporal asynchronous sharp and slow discharges

L = left; R = right; T = temporal; m = mesial; P = parietal; O = occipital; TPOJ = temporoparieto-occipital junction.

diffuse hypoperfusion involving the left frontal, parietal and temporal lobes, maximal in the posterior temporal ROI (AIs -13.9%, -13.8% and -16.0% in the lateral frontal, parietal and posterior temporal ROIs, respectively). Patient 2 had a localized area of hypoperfusion consistent with his MRI lesion. Interictal perfusion was normal in Patients 3 and 5.

Three patterns of ictal hyperperfusion were seen:

1. Hyperperfusion of the temporoparieto-occipital junction on the side of EEG seizure onset, extending into the ipsilateral lateral temporal cortex, with lesser hyperperfusion of the mesial temporal cortex and basal ganglia, and a small area of hyperperfusion in the contralateral parietal lobe. This pattern was seen in Patients 1 and 4 and is illustrated in Figure 1.
2. Hyperperfusion of the temporoparieto-occipital junction on the side of EEG seizure onset, extending into the lateral temporal cortex, with a small area of hyperperfusion of the contralateral parietal lobe. No hyperperfusion of the mesial temporal cortex or basal ganglia. This pattern was seen in Patient 5 and is illustrated in Figure 2.
3. Isolated and localized hyperperfusion of the temporoparieto-occipital junction on the side of EEG seizure onset. This pattern was seen in Patients 2 and 3 and is illustrated in Figure 3.

Four patients (1, 2, 4 and 5) also showed widespread ictal hypoperfusion of the hemisphere ipsilateral to seizure onset, excepting the hyperperfused areas mentioned previously.

Changes at the TPOJ in AI with respect to interictal figures were 40.9% (Patient 1), 18% (Patient 2), 33% (Patient 3), 59% (Patient 4) and 56.0% (Patient 5). The hyperperfusion was visually most impressive in Patient 5, where it involved a large area around the temporoparieto-occipital junction seizures, extending into adjacent parietal, occipital and temporal areas (Fig. 2A, B).

In Patients 1 and 5, ictal hypoperfusion was maximal in the inferior lateral frontal ROI, which was placed just anterior to the central sulcus in the area of the frontal operculum, with AI changes -38.3% and -23.3%, respectively. In Patient 4, the hypoperfusion was maximal in the superior lateral frontal ROI, with an AI change to -18.1%. Patient 3 showed a change to -18.1% in the intermediate lateral frontal ROI, which was not noted visually.

Patient 1 (Fig. 1A, B) demonstrated the most marked hyperperfusion of mesial structures, with ictal changes in mesial and lateral temporal AIs of 23.2% and 10.0%, respectively (bearing in mind that the latter figure was relative to an interictal anterior lateral temporal AI of 12.4 mentioned above). Patients 2 and 3 showed relatively small changes, of -3.4 and 0.1%, respectively, while Patient 4 showed a change of 9.4%, in keeping with the increase in perfusion noted visually. No mesial temporal changes were detected visually in these three patients. Patient 5 was visually reported to have ictal hypoperfusion of the mesial temporal cortex, and this was associated with -15.1% change in AI.

DISCUSSION

In all of our patients, the ictal patterns of perfusion were distinguished from those seen in mesial temporal seizures in that the hyperperfusion was clearly maximal in the temporoparieto-occipital junction. The perfusion patterns in

TABLE 1
Continued

Ictal EG		Interictal SPECT	Ictal SPECT	
Onset	Distribution		Injection time	Abnormality
L TP flattening	L then R temporo-parietal polyspikes	L TPO hyperperfusion LmT hyperperfusion	55 sec after onset	Hyperperfusion L lat. TPOJ extending into anterior lateral greater than mesial temporal lobe and basal ganglia hypoperfusion of rest of L hemisphere small area of hyperperfusion L parietal lobe
L posterior T flattening	L posterior T fast discharge	Focal deficit at TPOJ	28 sec after termination	L PTOJ hyperperfusion hypoperfusion of rest of L hemisphere
L TO flattening	L TO spikes then PO spikes, then R TO spikes	Normal	38 sec after onset	localized L TPOJ hyperperfusion
R TO fast spikes	R then L TO fast spikes	R hemispheric hypoperfusion	62 sec after onset	R TPOJ hyperperfusion extending into lateral greater than mesial temporal lobe and basal ganglia hypoperfusion of rest of R hemisphere Small area of hyperperfusion L parietal lobe
L posterior temporal spike discharge	L then R posterior temporal spike discharge	normal	35 sec after onset	Massive hyperperfusion of L TPOJ and surrounding areas, extending into lat temporal cortex hypoperfusion of rest of L hemisphere, including mesial temporal lobe small area of hyperperfusion in R parietal lobe

L = left; R = right; T = temporal; m = mesial; P = parietal; O = occipital; TPOJ = temporoparieto-occipital junction.

TABLE 2
Ictal Changes in Asymmetry Index (AI) with Respect to Interictal AI*

	Patient no.				
	1	2	3	4	5
	Side of EEG onset				
	L	L	L	R	L
ROI					
Med frontal	−23.6	2.8	−5.1	−4.2	−6.3
Sup lat frontal	−20.8	−10.5	−10.6	−18.1	−15.7
Int lat frontal	−38.3	−7.9	−18.1	−0.6	−23.3
Inf lat frontal	−30.4	−8.1	−9.6	−0.5	−16.0
Basal ganglia	1.9	0.8	13.2	−12.1	0.7
Med temporal	23.2	−3.4	0.1	9.4	−15.1
Ant lat temp	10.0	−11.4	0.5	8.4	24.4
Sup post temp	−26.3	−3.5	−1.9	−4.5	25.7
Inf post temp	−22.9	−8.4	8.8	−10.0	15.1
Parietal	−34.2	−6.6	8.9	−13.6	3.2
Calcarine	−13.6	0.3	2.2	−1.1	−9.0
Lat occipital	−20.1	−4.3	2.7	16.3	1.1
Cerebellum	−18.9	−1.7	0.3	−6.7	−1.8
TPOJ	40.9	18.0	33.0	59.0	56.0

*Polarity of changes is given with respect to the side of the EEG onset (i.e., changes are positive when there has been an increase in counts on the side of the EEG onset change and negative when there has been a decrease on the side of EEG onset.

Patients 1 and 4 bore the most similarity to that of a mesial temporal seizure (illustrated in Fig. 4), in that the mesial structures were hyperperfused as were, to some extent, the ipsilateral basal ganglia. The two main differences picked out by the observers, however, were the existence of an intense area of hyperperfusion in the area of the temporoparieto-occipital junction seizures and an unusual preponderance of lateral and polar versus medial temporal hyperperfusion more anteriorly [there is a slight preponderance of lateral temporal signal during mesial temporal seizures using some imaging systems (*3*)]. It

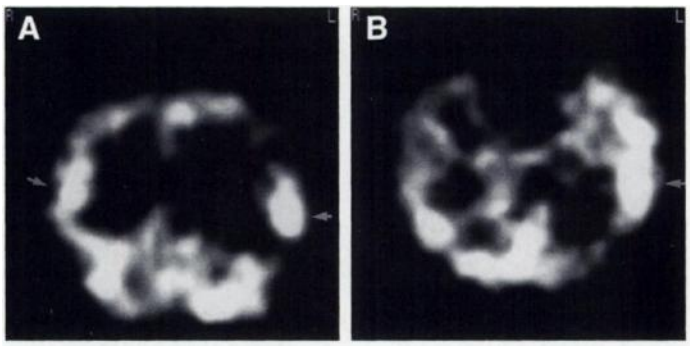

FIGURE 1. Patient 1. Posterior coronal slice shows localized but intense hyperperfusion in the area of the temporoparieto-occipital junction on the left (arrow, A). Note the small area of hyperperfusion in the right parietal cortex (arrow). Same dataset as in Figure 1A, but resliced to show axial views oriented in the plane of the long axis of the temporal lobe (B). There is hyperperfusion involving all temporal structures, but it is most intense at its posterior margin near the temporoparieto-occipital junction seizures (arrow).

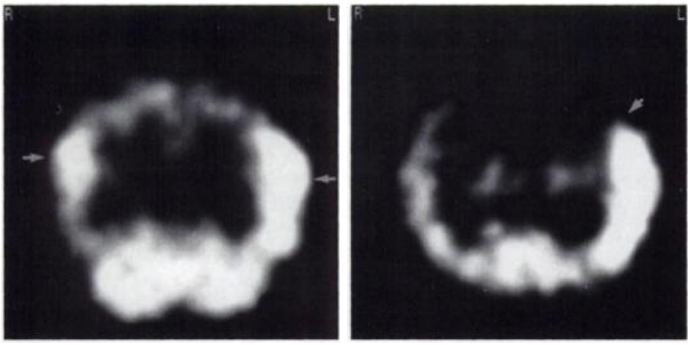

FIGURE 2. Patient 5. Posterior coronal slice shows hyperperfusion involving the posterior temporal, inferior parietal and anterolateral occipital cortex on the left (arrow), with a small, less intense and superiorly placed area of hyperperfusion on the right (arrow, A). Ictal change in AI was 40.9% in the area of the temporoparieto-occipital junction. Same dataset as Figure 2A, but resliced to show axial views oriented in the plane of the long axis of the temporal lobe. Note the slight relative hypoperfusion of ipsilateral anteromesial temporal structures (arrow, B).

might be argued that the lateral over mesial preponderance seen in the present study was due to attenuation effects, but the reconstruction parameters used in this study usually produce a signal difference of 15% in count density between mesial and lateral temporal lobe (see Fig. 4). The difference on the ictal image in Patient 1 was 53%.

Ictal hyperperfusion persisting for periods of days has been documented (*25*) and may be the cause of apparently interictal (by EEG and clinical definition) hyperperfusion observed in some studies (*26*). In this study, interictal HMPAO injections were not administered with EEG leads on and, although there was no clinical evidence of seizure activity at the time, this could not be entirely ruled out as a cause of apparent interictal hyperperfusion in Patient 1.

Major contralateral propagation of the seizure discharge was seen on EEG in all five patients in the present series. Evidence of contralateral hyperperfusion was seen on SPECT in three. In all patients, the contralateral activated area was small and placed in the parietal lobe, higher than the site of major activation on the side of seizure onset. Three of five patients showed extensive hyperperfusion of the ipsilateral lateral temporal cortex anterior to the temporoparieto-occipital junction seizures. This was consistent with anterior spread of ictal EEG discharges seen as the seizure progressed. Patients 1 and 4

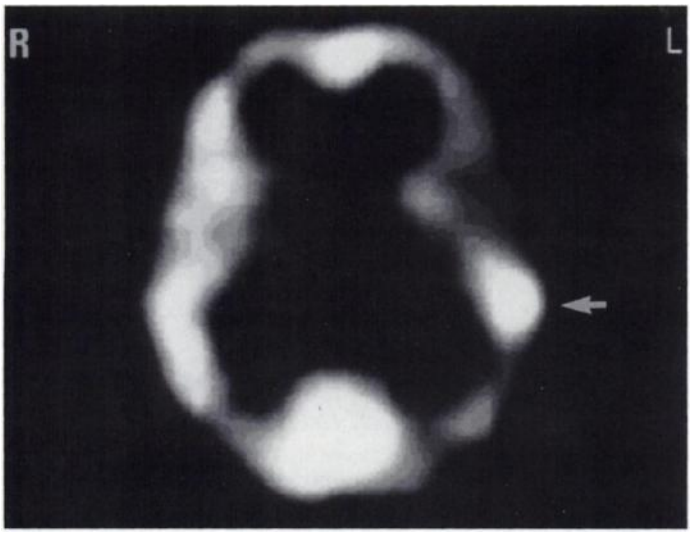

FIGURE 3. Patient 2. Axial slice in the orbitomeatal plane shows hyperperfusion in the area of the left temporoparieto-occipital junction (arrow) with hypoperfusion of the rest of the ipsilateral hemisphere.

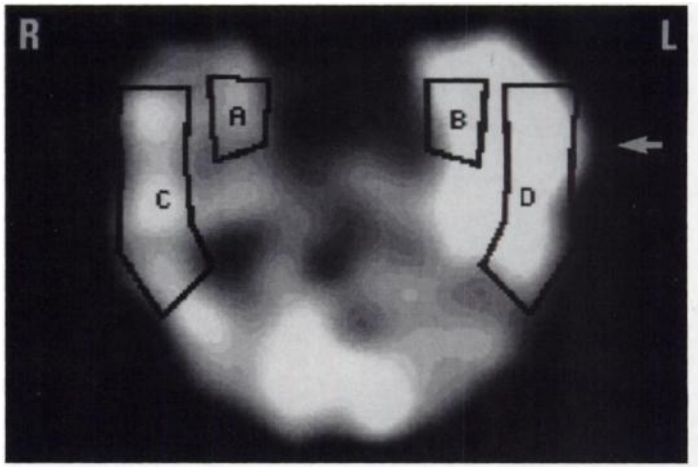

FIGURE 4. Ictal HMPAO-SPECT axial slice in the long-axis of the temporal lobe. Dataset was acquired with the same gamma camera used for the five patients in the present study. This temporal lobe slice illustrates the pattern of perfusion seen in previous studies of mesial temporal lobe seizures (*2,3,8,11*), i.e., hyperperfusion of the whole temporal lobe (arrow), which is displayed for purposes of comparison with the present series. As measured using the ROIs shown (the same as those used to analyze the datasets for the five patients in the present study), the left lateral temporal signal level was 13.8% more than the left mesial temporal signal level. This can be compared with the mesial-lateral difference of 53% in Patient 1.

showed activation of the mesial temporal cortex and had hyperperfusion of the basal ganglia. In contrast, both mesial temporal cortex and basal ganglia were relatively hypoperfused in Patient 5. The connectivity of mesial temporal structures, particularly the amygdaloid nucleus, with the basal ganglia is well-recognized (*27*). This may explain ictal dystonia in mesial temporal seizures (*13*), although careful examination of the seizure videos in Patients 1 and 4 showed no evidence of dystonic posturing.

Since clinical, imaging and noninvasive EEG data suggested seizure origin in the area of the temporoparieto-occipital junction, our patients did not have invasive EEG confirmation of site of origin of their seizures, and so the data presented here should be evaluated with this in mind. Nonetheless, our patient group was distinguished from patients with mesial temporal lobe epilepsy (MTLE) by clear posterior surface ictal EEG onsets, semiological features suggesting involvement of posterolateral cortex and the absence of semiological features of MTLE. Their patterns of ictal perfusion also differed from those in MTLE.

CONCLUSION

Our study suggests a distinct pattern of ictal perfusion in patients with posterolateral ictal EEG onsets, whose major elements are hyperperfusion in the area of the temporoparieto-occipital junction seizures plus or minus hyperperfusion of ipsilateral temporal lobe structures, contralateral parietal hyperperfusion and ipsilateral hemispheric hyperperfusion. Further study of larger series is required, but the present data provide evidence that ictal SPECT may be useful in distinguishing seizures in the area of the temporoparieto-occipital junction seizures from mesial temporal seizures, thus averting inappropriate surgical treatment.

REFERENCES

1. Rowe CC, Berkovic SF, Sia STB, Bladin PF. Patterns of postictal blood flow in temporal lobe epilepsy: qualitative and quantitative findings. *Neurology* 1991;41:1096.
2. Berkovic SF, Newton MR, Rowe CC. Localization of epileptic foci using SPECT. In: Luders H, ed. *Epilepsy surgery*. New York: Raven Press; 1992:251–256.

3. Berkovic SF, Newton MR, Chiron C, Dulac O. Single-photon emission computed tomography. In: J Engel Jr, ed. *Surgical treatment of the epilepsies*, 2nd ed. New York: Raven Press; 1993:233–243.
4. Lee BI, Markand ON, Siddiqui AR, et al. Single-photon emission computed tomography brain imaging using N,N,N′-trimethyl-N′-(2 hydroxy-3-methyl-5-123I-iodobenzyl)-1,3-propanediamine 2 HCl (HIPDM): intractable complex partial seizures. *Neurology* 1986;36:1471–1476.
5. Lee BI, Markand ON, Wellman HN, et al. HIPDM single-photon emission computed tomography brain imaging in partial onset secondary generalized tonic-clonic seizures. *Epilepsia* 1987;28:305–311.
6. Lee BI, Markand ON, Wellman HN, et al. HIPDM-SPECT in patients with medically intractable complex partial seizures. *Arch Neurol* 1988;45:397–402.
7. Shen W, Lee BI, Park HM, et al. HIPDM-SPECT brain imaging in the presurgical evaluation of patients with intractable seizures. *J Nucl Med* 1990;31:1280–1284.
8. Duncan R, Patterson J, Roberts R, et al. Ictal/postictal SPECT in the presurgical localization of complex partial seizures. *J Neurol Neurosurg Psych* 1993;56:141–148.
9. Rowe CC, Berkovic SF, Austin M, et al. Postictal SPECT in epilepsy. *Lancet* 1989;1:389–390.
10. Rowe CC, Berkovic SF, Sia STB, et al. localization of epileptic foci with postictal single-photon emission computed tomography. *Ann Neurol* 1989;26:660–668.
11. Newton MR, Berkovic SF, Austin MC, et al. Postictal switch in blood flow distribution in temporal lobe seizures. *J Neurol Neurosurg Psych* 1992;55:891–894.
12. Newton MR, Austin MC, Chan JG, et al. Ictal SPECT using ^{99m}Tc-HMPAO: methods for rapid preparation and optimal deployment of tracer during spontaneous seizures. *J Nucl Med* 1993;34:666–670.
13. Newton MR, Berkovic SF, Austin MC, et al. Dystonia, clinical lateralization and regional blood flow changes in temporal lobe seizures. *Neurology* 1992;42:371–377.
14. Harvey AS, Rowe JM, Hopkins IJ, et al. Ictal ^{99m}Tc-HMPAO SPECT in children with temporal lobe epilepsy. *Epilepsia* 1993;34:869–877.
15. Marks DA, Katz A, Hoffer P, Spencer SS. Localization of extratemporal epileptic foci during ictal single-photon emission computed tomography. *Ann Neurol* 1992;31:250–255.
16. Harvey AS, Hopkins IJ, Rowe JM, et al. Frontal lobe epilepsy: clinical seizure characteristics and localization with ictal ^{99m}Tc-HMPAO SPECT. *Neurology* 1993; 43:1966–1980.
17. Stefan H, Bauer J, Feistel H, et al. Regional cerebral blood flow during focal seizures of temporal and fronto central onset. *Ann Neurol* 1990;27:162–166.
18. Ho SS, Berkovic SF, Newton MR, et al. Ictal ^{99m}Tc-HMPAO SPECT findings in parietal lobe epilepsy. *Epilepsia* 1993;34(suppl 2):112.
19. Newton MR, Berkovic SF, Austin MC, et al. SPECT in the localization of extratemporal and temporal seizure foci. *J Neurol Neurosurg Psych* 1995;59:26–30.
20. Sveinbjornsdottir S, Duncan J. Parietal and occipital lobe epilepsy: a review. *Epilepsia* 1993;34:493–521.
21. Koelmel HW. Complex visual hallucinations in the hemianopic field. *J Neurol Neurosurg Psych* 1985;48:29–38.
22. Haecan H, Penfield W, Bertrand C, Malmo R. The syndrome of apractognosia due to lesions of the minor hemisphere. *Arch Neurol Psychiatr* 1956;75:400–434.
23. Wyllie E, Luders H, Morris HH, et al. The lateralizing significance of versive head and eye movements during epileptic seizures. *Neurology* 1986;36:606–611.
24. Bancaud J. Clinical semiology of seizures of temporal origin. *Rev Neurol* 1987;143: 392–400.
25. Podreka I, Lang W, Suess E, et al. HMPAO-SPECT in epilepsy. *Brain Topography* 1988;1:55–60.
26. Duncan R, Patterson J, Bone I, et al. Technetium-99m-HMPAO SPECT in temporal lobe epilepsy. *Acta Neurol Scand* 1990;81:287–293.
27. Alheid GF, Heimer L. New perspectives in basal forebrain organisation of special relevance for neuropsychiatric disorders: the striatopallidal, amygdaloid and corticopetal components of the substantia innominata. *Neuroscience* 1988;27:1039.

Dobutamine Thallium-201 SPECT Imaging for Assessment of Peri-Infarction and Remote Myocardial Ischemia

Abdou Elhendy, Jan H. Cornel, Jos R.T.C. Roelandt, Ron T. van Domburg, Marcel L. Geleijnse, Peter A.J. Hoeymans, Ambroos E.M. Reijs, Folkert J. TenCate, M. Moshen Ibrahim and Paolo M. Fioretti

Thoraxcenter and Department of Nuclear Medicine, University Hospital Rotterdam-Dijkzigt; Erasmus University, Rotterdam, The Netherlands; and Department of Cardiology, Cairo University Hospital, Cairo, Egypt

This study assessed the value of dobutamine ^{201}Tl scintigraphy for detecting significant disease of infarct-related and remote coronary arteries in myocardial infarction patients. **Methods:** Dobutamine (up to 40 μg/kg/min)/atropine (up to 1 mg) stress test in conjunction with stress-reinjection ^{201}Tl SPECT was performed in 71 symptomatic patients with left ventricular dysfunction >3 mo after myocardial infarction. Ischemia was defined as reversible perfusion defects. **Results:** Significant coronary artery stenosis (≥50% luminal diameter stenosis) was detected in all patients. Sensitivity, specificity and accuracy of regional ischemia for the diagnosis of remote coronary artery stenosis were 74% (95% CI 63–86), 80% (CI 70–90) and 76% (CI 65–87), respectively. Those for infarct-related artery stenosis were 71% (CI 60–81), 83% (CI 75–92) and 72% (CI 61–82), respectively. Ischemic perfusion score was higher in patients with multi- versus single-vessel disease (1056 ± 1021 versus 423 ± 633, $p < 0.01$). **Conclusion:** Dobutamine thallium scintigraphy is valuable for assessing the extent of coronary stenosis on the basis of reversible hypoperfusion in symptomatic patients late after myocardial infarction.

Key Words: dobutamine stress test; thallium-201 SPECT; myocardial infarction

J Nucl Med 1996; 37:1951–1956

Received Jan. 25, 1996; revision accepted Apr. 10, 1996.

For correspondence or reprints contact: Paolo M. Fioretti, MD, PhD, Thoraxcenter, Ba 300, Dr Molewaterplein 40, 3015 GD Rotterdam, The Netherlands.

Exercise ^{201}Tl perfusion scintigraphy is a widely used technique for the diagnosis and functional assessment of coronary artery disease (*1–4*). The presence of scintigraphic markers of myocardial ischemia after myocardial infarction, based on reversible hypoperfusion, is a predictor of future cardiac events (*3,4*).

Since exercise tolerance may be reduced in patients with left ventricular dysfunction, dobutamine stress testing represents a feasible and safe alternative (*5–11*). However, in the presence of severe myocardial dysfunction and severe perfusion abnormalities at rest, the detection of reversible perfusion defects represents a technical challenge for thallium scintigraphic techniques (*12,13*). Conversely, a study of patients after a recent myocardial infarction has shown that the prevalence of ischemia on dobutamine thallium scintigraphy is higher in peri-infarction compared to remote regions subtended with stenotic coronary arteries (*14*). Accordingly, we attempted to assess the value of dobutamine ^{201}Tl SPECT imaging for the diagnosis of infarct-related and remote coronary artery disease in symptomatic patients with left ventricular dysfunction late after acute myocardial infarction based on the presence of reversible hypoperfusion. We also wanted to assess the extent to which the severity of persistent perfusion abnormalities influence the occurrence of an ischemic response in individual myocardial regions subtended with stenotic coronary arteries.